NUMERICAL SIMULATION OF HEAT EXCHANGER

CONF-8509122--1

DE85 015002

William T. Sha
Argonne National Laboratory
9700 South Cass Avenue
Argonne, Illinois, U.S.A. 60439

1. INTRODUCTION

Accurate and detailed knowledge of the fluid flow field and thermal distribution inside a heat exchanger becomes invaluable as a large, efficient, and reliable unit is sought. This information is needed to provide proper evaluation of the thermal and structural performance characteristics of a heat exchanger. Thermal-hydraulically unbalanced design or operation of a heat exchanger often causes unequal thermal loadings among the heat-transfer tubes, which may result in excessive thermal stresses in the tube bundle, thus impacting upon the structural integrity and reliability of the unit. The structural integrity of the pressure-bearing boundaries of heat exchangers employed in nuclear reactor systems has direct reactor safety implications.

The flow pattern and the thermal map of a shell-and-tube heat exchanger may be obtained either through actual testing of a scale model or by using an analytical prediction method. Scale-model testing is, in general, very expensive, and requires a long lead time. Often instrumentation used in experiments must be able to withstand high temperature, high pressure, and a corrosive environment. Another problem associated with scale-model testing is that suitable similarity parameters must be obtained and matched between the scale model and the actual unit; otherwise all the conclusions and information drawn from the experimental data will be of limited value. Finally, both changing and upgrading the design of heat exchangers often are done routinely. If the design of a heat exchanger relies solely on experimental information, any significant deviation from the original design will require all tests to be repeated. This is a costly and time-consuming process.

It is to be noted that an analytical prediction method, when properly validated, will greatly reduce the need for model testing, facilitate interpolating and extrapolating test data, aid in optimizing heat-exchanger design and performance, and provide scaling capability. Thus tremendous savings of cost and time are realized. With the advent of large digital computers and advances in the development of computational fluid mechanics[1-3], it has become possible to predict analytically, through numerical solution, the conservation equations of mass, momentum, and energy for both the shellside and tubeside fluids. The numerical modeling technique will be a valuble, cost-effective design tool for development of advanced heat exchangers.

In the past, investigations[4] have been made to obtain the flow distribution inside a heat exchanger through solutions of the continuum Navier-Stokes equations. The idea of using distributed resistance to simulate the presence

of heat-transfer tubes and baffle plates on the shell side of a heat exchanger was first introduced by Patankar and Spalding[2]. These authors assumed that the space inside a heat exchanger is uniformly filled with fluid, throughout which, however, a resistance to fluid motion is distributed on a fine scale, but they did not calculate tubeside flow distribution. More recently, AbuRomia et al.[5] applied the distributed resistance concept to obtain the flow field between the typical tube support spans of the Clinch River Breeder Reactor Plant (CRBRP) intermediate heat exchangers. This analysis was limited to an isothermal flow field and included a turbulence model that is perhaps not appropriate for a tube bundle.

Recently a new porous-media formulation[6-10] was developed; it is rigorously derived through local volume averaging. The new porous-media formulation uses the concepts of volume porosity, directional surface porosities*, distributed resistance, and distributed heat source or sink. All past analyses utilized the conventional porous-media formulation, in which only volume porosity, distributed resistance, and distributed heat source are used. Volume porosity is defined as the ratio of the volume occupied by fluid in a control volume to the total control volume. Directional surface porosities are similarly defined as the ratio of flow area of a control surface to the total control surface in each principal coordinate direction. The concept of **directional surface porosities is new.** In thermal-hydraulic analysis, resistance (friction factor) is, in general, not known precisely for most engineering applications; directional surface porosities are a function of geometry and are known precisely. The new porous-media formulation uses both distributed resistance and directional surface porosities for modeling velocity and temperature fields in anisotropic media. This is in contrast with the conventional porous media, in which only the distributed resistance is used. Thus, any error in estimating resistance will not be reflected entirely in the results using the new porous-media formulations, but will be in the conventional porous-media formulation. The concept of directional surface porosities greatly facilitates modeling velocity and temperature fields in anisotropic media and, in general, improves resolution and accuracy. It may be noted that, without the volumetric porosity and directional surface porosities, the calculated fluid momentum would be lower than the actual momentum; and without the distributed resistance, the calculated pressure drop would be less than the actual pressure drop.

2. POROUS MEDIA FORMULATION VIA LOCAL VOLUME AVERAGE

In general, fluid flow and heat transfer in a heat exchanger are complex. The complication arises from the fact that the flow domain of interest often contains both irregularly shaped fluids, such as bubbles, and solid structures. The cost of detailed thermal-hydraulic analysis with explicit treatment of these structures often is prohibitive, if not impossible. An alternative is to capture the essential features of the system and to express the flow and temperature field in terms of locally global quantities while sacrificing some of the details. Often, this is all that is required in most engineering applications. The present work is an attempt to achieve this goal by applying the local volume-averaging technique. In the course of derivations, fundamental averaging theorems and their basic premises are reconsidered.

Attention is focused on single-phase flows in a domain containing dispersed but stationary heat-generating or heat-absorbing solid structures. Local

---

*In all our previous works, directional surface permeabilities instead of directional surface porosities are used.

volume-averaged governing equations--i.e., conservation of mass, momentum, and energy--and interface relations between fluid and solid structures for such a system are derived. Extension of the resultant set of single-phase conservation equations to a multiphase system has been carried out and presented elsewhere[9,10].

2.1 Averaging Relations

Consideration is hereby given to a domain consisting of a single-phase fluid and dispersed, stationary solid structures. Heat may be generated or absorbed by the structures. For an arbitrary point in the domain, we associate a closed surface A whose volume is V. A portion of V that contains the fluid is V_f and the total fluid-solid interface is A_{fs}. A portion of A through which the fluid may flow is A_e. A schematic of the system just described is illustrated in Fig. 1.

Local volume average, intrinsic average, and area average. Let ψ be any intensive property associated with the fluid. It may be a scalar, vector, or second-order tensor. The local volume average of ψ is defined by

$$^3\langle\psi\rangle = \frac{1}{V}\int_V I(p)\,\psi\,dV \qquad (1)^*$$

where p is the position vector and the indicator function, $I(p)$, is defined by

$$I(p) = \begin{cases} 1, & \text{if the end point of p is in fluid} \\ 0, & \text{if the end point of p is in solid} \end{cases} \qquad (2)$$

An equivalent form of Eq. (1) is

$$^3\langle\psi\rangle = \frac{1}{V}\int_{V_f}\psi\,dV \qquad (1a)$$

The intrinsic local volume average of ψ is

*The superscript 3 designates that the average is associated with volume; superscript 2 is used for area and line (segment) averages.

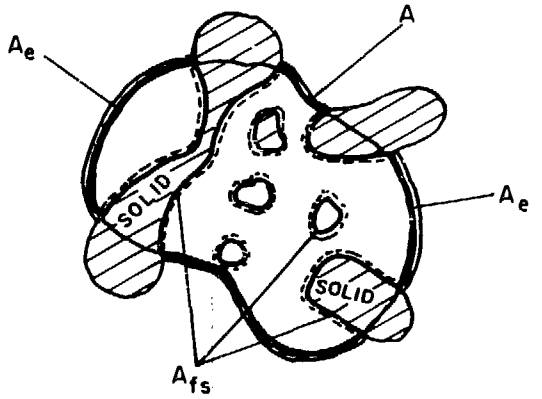

FIGURE 1. Local volume averaging of physical system.

$$^{3i}\langle\psi\rangle = \frac{1}{V_f}\int_{V_f} \psi\, dV \qquad (3)^*$$

Likewise, the local area average of ψ is

$$^{2}\langle\psi\rangle = \frac{1}{A}\int_{A} I(p)\,\psi\, dA = \frac{1}{A}\int_{A_f} \psi\, dA \qquad (4)$$

where A_f denotes the portion of A that is occupied by the fluid. The associated intrinsic area average is

$$^{2i}\langle\psi\rangle = \frac{1}{A_f}\int_{A_f} \psi\, dA \qquad (5)$$

It is important to note that in Eq. (4) the area A under consideration may <u>not</u> be the total enclosing surface. (If A is the enclosing surface in its entirety, then A_f in Eqs. (4) and (5) should be replaced by A_e; see Fig. 1.) In fact, one is often concerned with a designated portion of it. For instance, in the Cartesian-coordinate system, the averaging volume may be selected to be a parallelepiped $\Delta x\Delta y\Delta z$. The average mass flux through the surface ΔA_x (area $\Delta y\Delta z$) whose normal points in the direction of positive x axis is

$$^{2(x)}\langle\rho u\rangle = \frac{1}{\Delta A_x}\int_{\Delta A_x} I\,(p)\rho\, u\, dA$$

$$= \frac{1}{\Delta A_x}\int_{\Delta A_{x,f}} \rho\, u\, dA \qquad (4a)$$

where $\Delta A_{x,f}$ denotes the fluid portion of ΔA_x, ρ is the fluid density, and u is the fluid velocity in x direction. The corresponding intrinsic average is

$$^{2i(x)}\langle\rho u\rangle = \frac{1}{\Delta A_{x,f}}\int_{\Delta A_{x,f}} \rho\, u\, dA \qquad (5a)$$

<u>Volume porosity and directional surface porosities.</u> The ratio of fluid volume V_f to the total volume V is defined to be the volume porosity, γ_v. Thus,

$$\gamma_v = \frac{V_f}{V} \qquad (6)$$

Since $V_f = \int_V I(p)dV$, γ_v can also be written as

$$\gamma_v = \frac{1}{V}\int_V I(p)dV \qquad (6a)$$

---

*The superscript i denotes intrinsic average.

Furthermore,

$$^{3}\langle\psi\rangle = \gamma_{v}\ ^{3i}\langle\psi\rangle \tag{7}$$

Analogously, we define the surface porosity γ_A associated with any surface (not necessarily closed) as

$$\gamma_A = \frac{A_f}{A} = \frac{1}{A}\int_A I(\mathbf{p})dA \tag{8}$$

where A_f is the portion of A that is occupied by the fluid. Consider, for example, the surface ΔA_x described in the section titled "Local volume average, intrinsic average, and area average." Its directional surface porosity in the x direction is

$$\gamma_{A_x} = \frac{\Delta A_{x,f}}{\Delta A_x} = \frac{1}{\Delta A_x}\int_{\Delta A_x} I(\mathbf{p})dA \tag{9}$$

Clearly,

$$^{2}\langle\psi\rangle = \gamma_A\ ^{2i}\langle\psi\rangle \tag{10}$$

Local volume-averaging theorems. The volume averages of derivatives of ψ are given by the local volume-averaging theorems as[11,12,13,14]

$$^{3}\langle\nabla\psi\rangle = \nabla\ ^{3}\langle\psi\rangle + V^{-1}\int_{A_{fs}} \psi\ \mathbf{n}\ dA \tag{11}$$

$$^{3}\langle\nabla\cdot\psi\rangle = \nabla\cdot\ ^{3}\langle\psi\rangle + V^{-1}\int_{A_{fs}} \boldsymbol{\psi}\cdot\mathbf{n}\ dA \tag{12}$$

and

$$^{3}\langle\partial\psi/\partial t\rangle = \partial\ ^{3}\langle\psi\rangle/\partial t - V^{-1}\int_{A_{fs}} \psi\mathbf{v}\cdot\mathbf{n}\ dA \tag{13}$$

Note that these averaging relations are subject to the restriction that [13]

(Characteristic length of pores and phases)

$\ll$ (characteristic length of averaging volume)

$\ll$ (characteristic length of the physical system). (14)

The averaging volume under consideration, therefore, cannot be arbitrarily small or become infinitesimal.

2.2 Local Volume-Averaged Conservation Equations

By using the local volume averaging theorems as shown in the previous section, the resultant local volume averaged conservation of mass, momentum and

enthalpy equation may be summarized as follows. The detailed derivation of those averaged equations can be found in Ref. 9.

Conservation of mass.

$$\gamma_v \frac{\partial {}^{3i}\langle\rho\rangle}{\partial t} + \frac{1}{V}\int_{A_e} \rho \mathbf{v} \cdot \mathbf{n} dA = 0 \tag{15}$$

where ρ = fluid density, t = time, and v = fluid velocity vector.

Conservation of momentum.

$$\gamma_v \frac{\partial}{\partial t} {}^{3i}\langle\rho \mathbf{v}\rangle + \frac{1}{V}\int_{A_e} \rho \mathbf{v} (\mathbf{v} \cdot \mathbf{n}) dA$$

$$= \gamma_v {}^{3i}\langle\rho\rangle \mathbf{g} - \gamma_v \nabla {}^{3i}\langle p\rangle + \frac{1}{V}\int_{A_e} \tau \cdot \mathbf{n} dA - \gamma_v {}^{3i}\langle \mathbf{R}\rangle \tag{16}$$

where g = gravitational acceleration vector, p = static pressure, τ = stress tensor, and R = distributed resistance which is defined as

$$-\int_{V_f} \mathbf{R} dV = \int_{A_{fs}} (-p\mathbf{n} + \tau \cdot \mathbf{n}) dA \tag{17}$$

Conservation of energy in terms of enthalpy.

$$\gamma_v \frac{\partial}{\partial t} {}^{3i}\langle\rho h\rangle + \frac{1}{V}\int_{A_e} \rho h \mathbf{v} \cdot \mathbf{n} dA$$

$$= \gamma_v {}^{3i}\frac{dp}{dt} + \frac{1}{V}\int_{A_e} k\mathbf{n} \cdot \nabla T dA$$

$$+ \gamma_v \left({}^{3i}\langle \dot{Q}_{rb}\rangle + {}^{3i}\langle \dot{Q}\rangle + {}^{3i}\langle\Phi\rangle \right) \tag{18}$$

where h = enthalpy, q = heat flux vector = $-k\nabla T$, k = thermal conductivity, T = temperature, $\dot{Q}_{rb}$ = rate of heat liberation from the dispersed solids per unit volume of the fluid, $\dot{Q}$ = rate of internal heat generation per unit fluid volume, and Φ = dissipation rate of mechanical energy into heat.

2.3 Reducing this new formulation to conventional Porous Media Formulation and Continuum

Equations (15, 16, and 18) form a set of local volume-averaged conservation equations and constitute a new porous media formulation. Directional surface

porosities will be brought out through finite-differencing the surface integrals of these equations. It can be shown readily that the conventional porous media formulation is a subset of the present formulation. Furthermore, the new porous media formulation can provide detailed and local velocity and temperature fields if the problems under consideration involve body shapes that do lend themselves to any one of the Cartesian, cylindrical, or spherical coordinate representations. Figure 2 shows that both the conventional porous media formulation and continuum are subsets of this new porous media formulation.

3. TURBULENCE MODELING

The turbulence model presented here is limited to single-phase applications. Two-phase or multiphase turbulence modeling is in its infancy and will not be discussed here. The turbulence model[15] developed and presented here is for quasicontinuum or porous media for the transport of momentum and heat in large tube bundles. This model utilizes the concepts of volume porosity, directional surface porosities, and distributed resistance. Although the model is relatively simple, it does take into account explicitly the effects of turbulent kinetic energy generation due to shear, viscosity, diffusion, geometric effects, buoyancy, and Reynolds number. This model is designed primarily for tube bundle analysis with a mesh size consisting of a number of tubes. The other models were developed for a continuum [16,17,18] and are more appropriate for use in the inlet and exit headers of a heat exchanger. They account for the transport effects of the turbulent kinetic energy k, turbulent kinetic energy dissipation rate ε, and scalar energy g. At any point in the flow, values for either k-ε-g of the three equation model, or k-ε of the two-equation model are obtained from transport-type equations. For the three-equation model [16,17], turbulent momentum fluxes (Reynolds stresses) and heat transport rates are obtained from an algebraic formulation containing k-ε-g, the mean velocities and temperatures, as well as their gradients. For the two-equation model[18], turbulent viscosity is calculated as a function of local k and ε. Both three-equation and two-equation turbulence models will not be presented here. Since most heat exchangers are cylindrical in form,

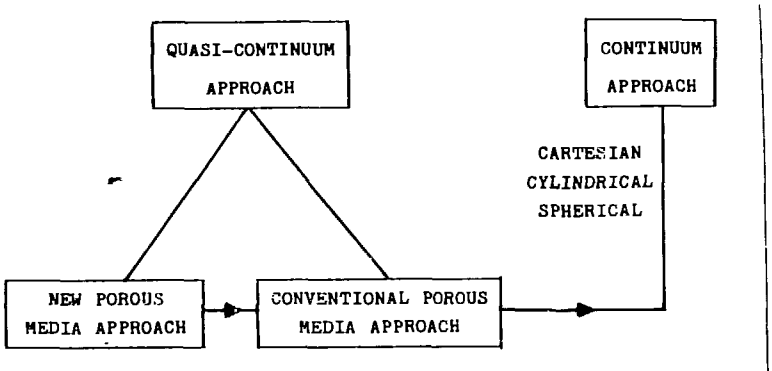

VOLUME POROSITY	γ_v	γ_v	$\gamma_v = 1$
DISTRIBUTED RESISTANCE	R_x, R_y, R_z	R_x, R_y, R_z	$R_x = R_y = R_z = 0$
DISTRIBUTED HEAT SOURCE (SINK)	q	q	q_{rb}
DIRECTIONAL SURFACE POROSITIES	$\gamma_x, \gamma_y, \gamma_z$	$\gamma_x = \gamma_y = \gamma_z = \gamma_v$	$\gamma_x = \gamma_y = \gamma_z = 1$

FIGURE 2. A unified approach to a fluid flow system.

cylindrical coordinates r, θ, and z are used for all the formulations presented below.

3.1 Quasi-Continuum Model — Turbulent Kinetic Energy (k) Equation

When the flow is turbulent, the transport equation for turbulent kinetic energy (k) may be written as:

$$\gamma_v \frac{\partial \rho k}{\partial t} + \nabla \cdot \gamma_A \rho \mathbf{v} k$$

$$= \gamma_v \{c_s \mu_t [(u - u_s)^2 + (v - v_s)^2 + (w - w_s)^2]/D_h^2$$

$$- \rho k^{3/2}/\ell\} + \gamma_v c_B \rho |U|^3 [(A_x/A_0) - 1]^2/\delta x$$

$$- \gamma_v \{[\hat{\alpha} (T - T_w) \beta g/c_p]/[1 + (\mu Pr_t)/(\mu_t Pr)]\} w_p^*/(\pi D_h)$$

$$+ \nabla \cdot \mu_{eff} \nabla \gamma_A k \qquad (19)$$

where

u,v,w = components of velocity vector $\mathbf{v}$

u_s, v_s, w_s = effective wall slip velocity components

A_x = cross sectional area of a computational cell upstream or downstream from the blockage

A_0 = Open area of a computational cell upstream or downstream from the blockage

U = velocity perpendicular to the baffle

w_p^* = heat transfer perimeter

D_h = equivalent hydraulic diameter

$\hat{\alpha}$ = heat transfer coefficient

T, T_w = mean fluid and wall temperature

μ, μ_t = molecular and turbulent viscosity

Pr, Pr_t = molecular and turbulent Prandtl number

β = dimensionless volumetric expansion coefficient

g = gravitational acceleration

and

c_p = specific heat at constant pressure.

The detailed derivation of Eq. 19 can be found in Ref 15. The effective viscosity μ_{eff} is given by

$$\mu_{eff} = \mu_t + \mu = c_\mu \rho k^{1/2} \ell + \mu \tag{20}$$

where

$$c_\mu = c_{\mu\infty} \quad \text{for } Re_{max} > 2000$$

$$c_\mu = c_{\mu\infty}(0.001\ Re_{max} - 1) \quad \text{for } 10^3 \leq Re_{max} \leq 2 \times 10^3$$

$$c_\mu = 0 \quad \text{for } Re_{max} < 1000$$

and

Re_{max} is the maximum of Re_x, Re_y, and Re_z.

The length scale appearing in Eq. (20) and on the right-hand side of Eq. (19) is taken as linearly proportional to the hydraulic diameter of the tube; i.e.,

$$\ell = c_\ell D_h \tag{21}$$

where c_ℓ is a coefficient.

The turbulent Prandtl number is obtained from[19]

$$Pr_t = 0.8[\,1 - \exp(-6 \times 10^{-5} Re_{max} Pr^{1/3})\,]^{-1} \tag{22}$$

The various empirical coefficients appearing in the model are recommended to be assigned initial values as follows:

Quantity	Initial Value	Quantity	Initial Value
c_B	0.2	$c_{\mu\infty}$	0.1
c_ℓ	0.4	u_s	0.5u
c_R	0.4	v_s	0.5v
c_s	2.0	w_s	0.5w

4. NUMERICAL SOLUTION ON SHELL SIDE

Equations 15, 16, 18, and 19 constitute a set of governing equations on shell-side. These equations are finite differenced in a staggered mesh system and solved by the ICE technique with a set of appropriate initial and boundary conditions. The detailed finite difference equations and solution technique can be found in Refs. 3, 20, and 21.

5. SHELL- AND TUBE-SIDE HEAT TRANSFER COUPLING

The development of a computational procedure or a computer code that would be used in the design of large heat exchangers requires a model for the heat transfer that takes place between the shell-side fluid and the tube-side fluid. Such a heat transfer model incorporates the tube-side fluid, tube wall, and heat transfer between the shell-side and tube-side fluids.

5.1 Shell-Side Energy Equation

The shell-side energy equation as described in Eq. (18) will not be repeated here. It is sufficient to say that the energy equation contains a thermal sink (or source) term. This term accounts for the heat transfer either from the shell-side fluid to the tube wall, or from the tube wall to the shell-side fluid, and is a function of the number of tubes in the control volume, shell-side heat transfer coefficient, and surface heat transfer area.

5.2 Tube Wall Conduction Equation

For the tube wall, the temperature is given by

$$\rho_w c_{pw} \frac{dT_w}{dt} = \frac{T - T_w}{V R_o} A + \frac{T_t - T_w}{V R_i} A \tag{23}$$

where

ρ_w = tube material density,

c_{pw} = tube material specific heat,

R_o = heat transfer resistance between T and T_w,

R_i = heat transfer resistance between T_t and T_w,

T_t = tube-side fluid temperature,

A = heat transfer area

and

V = total volume of tubes.

The overall heat transfer resistances, R_o and R_i, consist of the various resistances associated with conduction through the tube material, convective resistance due to fluid motion, and any resistance due to fouling. These resistances are in series with each other, and so, are additive. They are generally calculated in some ad hoc manner. In this case, half of the thickness of the wall material was associated with the tube side, while the other half thickness was associated with the shell side to simplify computation.

5.3 Continuum Governing Equation on Tube Side

The flow distribution on the tube side of the heat exchanger is governed by the one-dimensional conservation equation. The assumptions employed in reducing the equation to one dimension and other specific simplifications are discussed in [22]. The equations are included here for completeness. The continuity and momentum equations, respectively, are

$$\frac{\partial \rho}{\partial t} + \frac{\partial}{\partial z}(\rho w) = 0 \tag{24}$$

and

$$\frac{\partial}{\partial t}(\rho w) + \frac{\partial}{\partial z}(\rho w^2) = -\frac{\partial p}{\partial z} + \rho g - \frac{f}{D}\left(\frac{1}{2}\rho w|w|\right) \tag{25}$$

where

z = axial coordinate,

t = time,

w = axial velocity,

ρ = density,

p = pressure,

g = axial body force,

μ = molecular viscosity,

f = pipe friction factor,

and

D = tube inner diameter.

The tube side energy equation is given as

$$\frac{\partial}{\partial t}(\rho h) + \frac{\partial}{\partial z}(\rho w h) = \frac{T_w - T_t}{R_i V} A + \frac{\partial}{\partial z}\left(\hat{k}\frac{\partial T_t}{\partial z}\right) \tag{26}$$

where h = enthalpy, A = heat transfer area, $\hat{k}$ = thermal conductivity, and subscript t denotes tube side.

6. SOME NUMERICAL SIMULATIONS

Equations (15, 16, 18, 24, 25, and 26) constitute a set of governing equations coupled with appropriate initial and boundary conditions. The coupling between shell side and tube side can also be viewed as a boundary condition either from the shell side or tube side point of view.

The following two numerical results presented were obtained from the COMMIX-IHX/SG code.[3,23] The COMMIX-IHX/SG code is a three-dimensional, steady-state/transient computer code for thermal-hydraulic analysis of heat exchangers and is developed primarily for LMFBR applications. The shell side is capable of handling single-phase sodium and the tube side is capable of treating either single-phase sodium or two-phase flow water. The detailed description of COMMIX-IHX/SG can be found in Refs. [3,23]. A comparison between COMMIX results and experimental data are summarized below.

6.1 30° Sector Full-size CRBRP Intermediate Heat Exchanger Flow Model Test

This is an isothermal flow model test conducted by Foster Wheeler Energy Corporation.[4] The 30° sector, full-scale test model duplicates the Clinch River Breeder Reactor Plant (CRBRP) intermediate sodium heat exchanger tube bundle configuration, including the tubes, baffles, and inner and outer shrouds. The model length, however, is shorter by three baffle spans than the corresponding IHX bundle. Figure 3 shows the tube bundle configuration and a vertical cross-sectional view of the experimental setup. The tube bundle has been assembled with 219 stainless steel tubes of 22-mm (7/8 in.) OD in an equilateral pitch of 33.3 mm (1.312 in.). The upper half of the bundle has 2/3 area overlapping baffles and the lower half contains 1/2 area overlapping baffles. Water at a temperature of 77°C (170°F) was used as a working fluid to simulate sodium viscosity and Reynolds number. The full flow rate for the model was 10.56 m^3/min (1790 gpm), which corresponds to the full flow rate of the CRBRP-IHX.

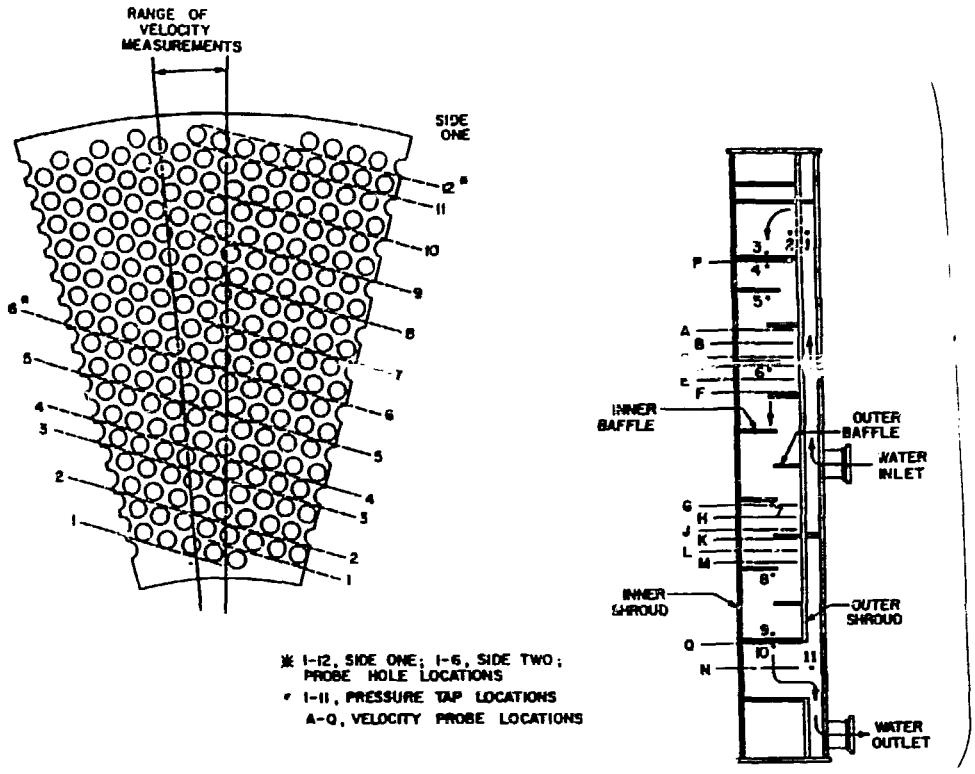

FIGURE 3. CRBRP-IHX tube bundle flow model.

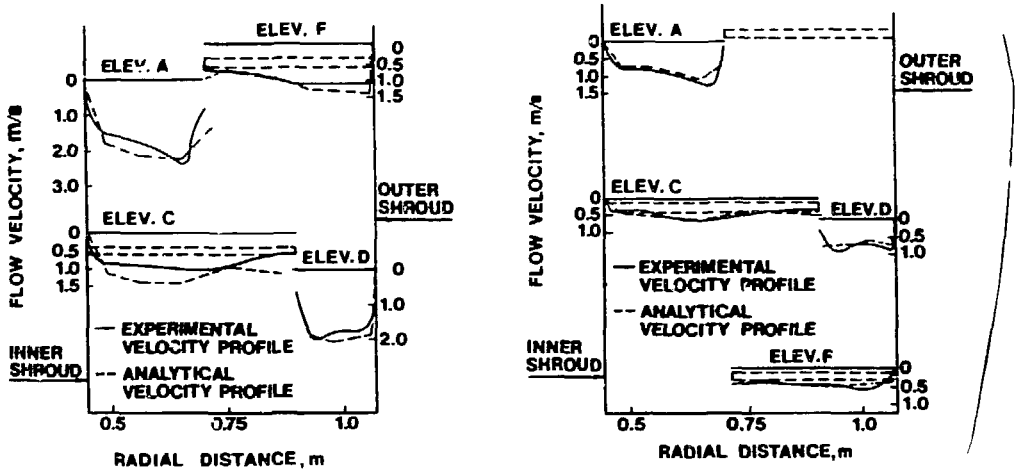

at 100% flow at 40% flow

FIGURE 4. Axial velocity profile.

The COMMIX-IHX/SG computer model of the above 30° sector IHX test module is a two-dimensional, axisymmetric one, consisting of 9 radial nodes and 76 axial nodes. Several computer runs were made with different inlet flow rates ranging from 100 to 10 percent of full flow. The results for the axial velocity components at various elevations near the flow baffles are shown in the broken lines in Fig. 4 for 100 and 40 percent of full flow conditions, respectively. Superimposed on these analytical velocity profiles are the corresponding

measured velocity profiles. The agreement between analytical predictions and experimental data appears satisfactory, considering experimental uncertainties and analytical complexities. At 100 percent flow rate, the analytical solution overestimates the axial velocity components, implying that the crossflow resistance correlation used in the analysis may be conservative. A comparison for the pressure drop across the test unit is shown in Fig. 5. The agreement is quite good, even though the analytical predictions tend to be higher at 100 percent flow, and lower at 10 percent flow, than the measurements.

6.2 AI Modular Steam Generator Test

The Atomics International Modular Steam generator (AI-MSG) is a counterflow, once-through, sodium-to-water heat exchanger with an inverted hockey stick configuration. Sodium flows downward on the shell side and water/steam flows upward inside 158 tubes. Sodium nozzles are located some distance away from water and steam nozzles, and semistagnant sodium regions exist in the tube bundle between the sodium outlet and the water inlet, and between the sodium inlet and the steam outlet. The physical dimensions of the MSG are summarized in Table 1. Further details of the MSG and its operation may be found in Ref. [24].

The COMMIX-IHX/SG computer model for the AI-MSG unit, shown in Fig. 6, is an axisymmetric model with 8 radial and 82 axial nodes, totaling 656 nodes. (See Fig. 7 for unit configuration.) The active heat-transfer region consists of axial nodes 11 through 73. The upper hockey-stick bend area is simulated by a vertical cylindrical section (nodes 1 through 10) because the present version of the code does not have provisions to model a bend or elbow configuration. The lower stagnation region is modeled by nodes 74 through 82. In the radial direction, the tube bundle is modeled by nodes 1 through 6. Radial node 7 simulated the tubeless space between the bundle and the shell.

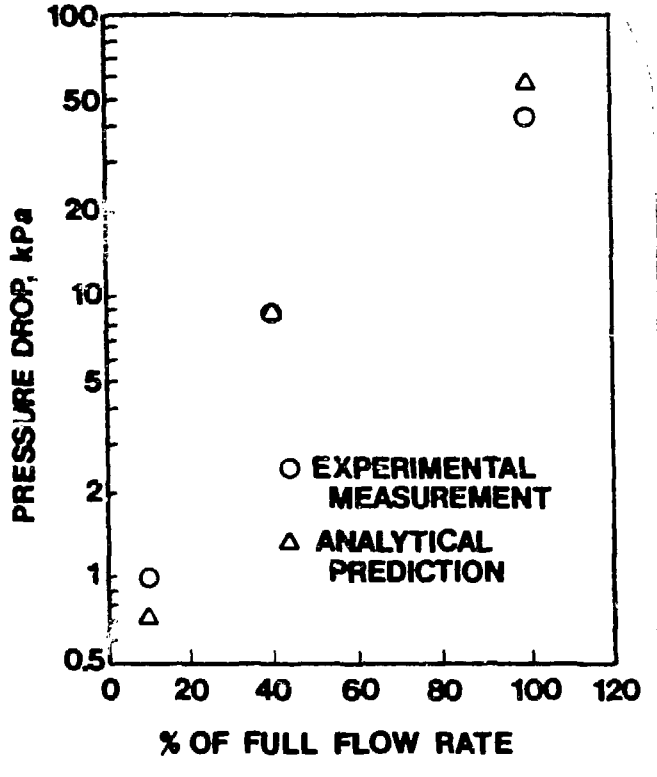

FIGURE 5. 30 degree sector model pressure drop.

TABLE 1. AI-MSG Physical Dimensions

Tubes	
Outside diameter (mm)	15.875
Tube wall thickness (mm)	2.921
Tube length (tubesheet to tubesheet)(m)	
Shortest tube	20.88
Longest tube	21.47
Active heat-transfer length (m)	17.68
Active heat-transfer area (m^2)	139.0
Number of tubes	158.0
Average pitch-to-diameter ratio	1.885
Material	2 1/4 Cr-1Mo steel
Tubesheets	
Thickness (mm)	152.4
Outside diameter (mm)	482.6
Shell	
Main shell outside diameter (mm)	457.2
Main shell thickness (mm)	19.05
Header shell outside diameter (mm)	609.6
Header shell thickness (mm)	50.8
Tube Spacers	
Thickness (mm)	19.05
Number of tube spacers	24.0
Support	8 tierods
Hole diameter (mm)	16.18

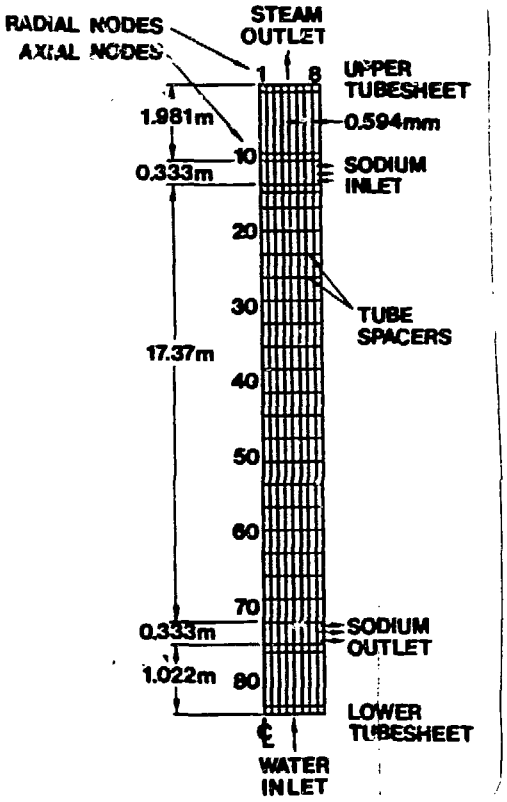

FIGURE 6. COMMIX model for modular steam generator.

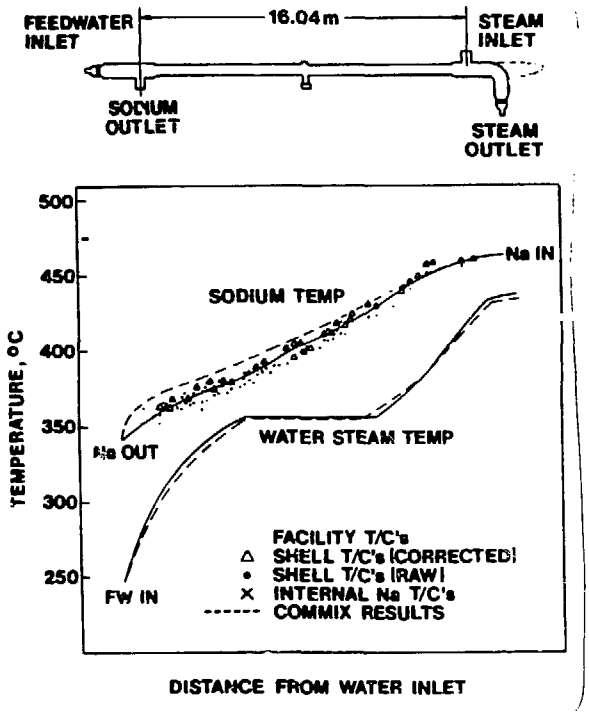

FIGURE 7. MSG performance data and COMMIX predictions.

TABLE 2. AI-MSG steady-state operation test conditions (102.8 percent power)

Water flow (kg/hr)	57,800
Sodium flow (kg/hr)	735,000
Water inlet temperature (°C)	246
Sodium inlet temperature (°C)	464
Steam outlet pressure (MPa)	17.9
Steam outlet temperature (°C)	439
Sodium outlet temperature (°C)	341
Thermal duty (MW)	32.1

The thermal hydraulic operating conditions used for the COMMIX-IHX/SG simulation model are summarized in Table 2. This steady-state condition corresponds to 102.8 percent power condition.

In the MSG test, thermocouples were mounted on the shell wall and inside the tube bundle. The thermocouple data points for Table 3 test conditions are shown in Fig. 7 as a function of the active heat-transfer length of the bundle. The solid line indicates the average temperature profile based on these thermocouple data. Superimposed on this, in broken lines, are the analytical results from the COMMIX-IHX/SG code. Fairly good agreement between the test data and predicted values is seen.

Also plotted in Fig. 7 are the average water/steam temperature profiles. Note that on the water/steam side, only the inlet water and outlet steam temperatures were measured by test facility thermocouples. The solid line water/steam temperature profile is computed based on the measured averaged sodium temperature along the steam generator. The discrepancy between the predicted exit steam temperature (435°C) and the measured value (439°C) is nearly within

TABLE 3. 50-MWt SNR-Steam Generator Physical Dimensions

Tubes	
Outside diameter (mm)	17.2
Tubewall thickness (mm)	2.9
Heating surface based on OD (m^2)	104.2
Active heat transfer tube length (m)	13.87
Number of tubes	139
Tube arrangement	Triangular
Tube pitch (mm)	27.5
Material	2 1/4 Cr-1Mo steel
Tube Spacer/Support	
Number of tube supports	20
Perforation	75%
Shell	
i.d. (mm)	468
Thickness (mm)	20

the experimental measurement error band of ±3°C that was estimated for the exit steam temperature. From a standpoint of enthalpy pickup by water/steam, the above discrepancy of 4°C for the exit steam temperature amounts to less than 0.3 percent difference.

The overall tube side pressure drop is computed to be 661 kPa, which compares favorably with the 669 kPa drop measured in the experiment.

7. DISCUSSIONS AND CONCLUSIONS

The detailed development of a comprehensive, multidimensional, thermal-hydraulic, heat-exchanger analysis computer code is presented. The concept of porosity, directional surface porosities, distributed flow resistance, and distributed heat source or sink has been employed on the shell-side fluid to modify the continuum Navier-Stokes and energy equations to properly account the blockage effects of the heat exchanger tube bundle. The tubeside flow is considered as a multichannel, parallel flow between two common inlet and exit plena. The conservation equations were put into finite-difference form using the implicit continuum-fluid Eulerian (ICE) method and solved on a digital computer.

The comparisons between analytical predictions and experimental indications (some of them are presented here) appear satisfactory, considering analytical complexities and experimental uncertainties, thus lending a credence to the analytical model. Numerical modeling of heat exchangers can be used for optimizing design, safety analysis, and scaling. However, there definitely is room for further improvement in the analytical approach.

ACKNOWLEDGEMENT

This paper is based on work which was supported by the U.S. Department of Energy under ANL Contract No. 31-109-38-381, Foster Wheeler Contract Nos. 8-33-3088 and 8-51-3864, and the U.S. Nuclear Regulatory Commission under Contract A-2045.

REFERENCES

1. Harlow, F. H. ed., *Computer Fluid Dynamics - Recent Advances*, AIAA Selected Reprint Series, XV, Feb. 1973.

2. Patankar, S. V., and Spalding, D. B., A Calculation Procedure for the Transient and Steady-State Behavior of Shell-and-Tube Heat Exchangers, in *Heat Exchangers: Design and Theory Sourcebook*, eds., N. H. Afgan and E. V. Schlunder, pp. 155-176, McGraw-Hill, 1974.

3. Sha, W. T., Kao, T. T., Yang, C. I., and Cho, S. M., Three-Dimensional Numerical Modeling of Heat Exchangers, *J. of Heat Transfer*, vol. 104, No. 3, pp. 397-573, Aug. 1982.

4. AbuRomia, M. M., Bosch, Jr., R. J., Cho, S. M., Dietz, D., and Jaisingh, G., Flow Model Test Development of CRBRP Intermediate Heat Exchanger, *Proc. ASME/IEEE Joint Power Generation Conference, Los Angeles*, ASME Paper No. 77-JPGC-NE-10, Sept. 18-21, 1977.

5. AbuRomia, M. M., Chao, B. C., and Cho, S. M., Flow Distribution Analysis in Nuclear Heat Exchangers with Applications to CRBRP-IHX, *Proc. of 1976 Heat Transfer and Fluid Mechanics Institute*, Stanford U. Press, pp. 468-482, 1976.

6. Sha, W. T., Domanus, H. M., Oras, J. J., and Lin, E. I. H., "COMMIX-1: A Three-Dimensional Transient Single-Phase Component Computer Program for Thermal Hydraulic Analysis," ANL Report ANL-77-96, NUREG/CR-0785, Sept. 1978.

7. Sha, W. T., Domanus, H. M., Schmitt, R. C., Oras, J. J., Lin, E. I. H., and Shah, V. L., A New Approach for Rod-Bundle Thermal-Hydraulic Analysis, *Proc. of the Int. Meeting on Nuclear Power Reactor Safety, Brussels, Belgium*, Oct. 16-19, 1978.

8. Sha, W. T., An Overview of Rod Bundle Thermal-Hydraulic Analysis, ANL Report ANL-79-10, NUREG/CR-1825, Nov. 1980.

9. Sha, W. T., Chao, B. T., and Soo, S. L., Local Volume-Averaged Transport Equations for Multiphase Flow in Regions Containing Distributed Solid Structures, ANL Report ANL-81-69, NUREG/CR-2354, Dec. 1981.

10. Sha, W. T., Chao, B. T., and Soo, S. L., Porous Media Formulation for Multiphase Flow with Heat Transfer, *Nuclear Engineering and Design*, vol. 82, pp. 93-106, October 1984.

11. Slattery, J. C., Flow of Viscoelastic Fluids through Porous Media, *AIChE J*, vol. 13, p. 1066, 1967.

12. Whitaker, S., Diffusion and Dispersion in Porous Media, *AIChE J.*, vol. 13, pp. 420-427, 1967.

13. Whitaker, S., Advances in Theory of Fluid Motion in Porous Media, *Ind. Eng. Chem.*, vol. 61, No. 12, p. 14, 1969.

14. Gary, W. G., and Lee, P. C. Y., On the Theorem for Local Volume Averaging of Multiphase System, *Int. J. of Multiphase Flow*, vol. 3, pp. 333-340, 1977.

15. Sha, W. T., and Launder, B. E., Internal Memorandum, January 1979.

16. Sha, W. T., and Launder, B. E., Internal Memorandum, March 1979.

17. Yang, C. I., and Sha, W. T., Numerical Modeling of Turbulent Flow in Pipes with Reynolds Stress Closure, *Proc. of Joint ASME/ASCE Mechanics Conference, Boulder, Colorado*, June 22-24, 1981.

18. Chen, F. F., Domanus, H. M., Sha, W. T., and Shah, V. L., Turbulence Modeling in the COMMIX Computer Code, ANL Report ANL-83-65, NUREG/CR-3504, EPRI NP-3546, April 1984.

19. Nijsing, R., and Eifler, W., Temperature Fields in Liquid Metal Cooled Assemblies, *Proc. Heat Mass Transfer*, vol. 7, p. 115, 1973.

20. Harlow, F. H., and Amsden, A. A., A Numerical Fluid Dynamics Calculation Method for All Flow Speeds, *J. Comp. Phy.*, vol. 8, pp. 197-213, 1976.

21. Sha, W. T., Domanus, H. M., Schmitt, R.C., Oras, J. J., and Lin, E. I. H., COMMIX-1: A Three Dimensional Transient Single-Phase Component Computer Program for Thermal Hydraulic Analysis, ANL Report ANL-77-96, NUREG/CR-0415, 1978.

22. Antonia, R. A., Dank, H. O., and Prabber, A., Response of a Turbulent Boundary Layer to a Step Change in Surface Heat Flux, *J. of Fluid Mech.*, vol. 80, No. 1, 1977.

23. Yang, C. I., Sha, W. T., and Kasza, K. E., Thermal-Hydraulic Posttest Analysis for the ANL/MCTF 360° Model Heat-Exchanger Water Test under Mixed Convection, *Proc. of 10th IMACS World Congress on Systems Simulation and Scientific Computation, Montreal, Canada*, Aug. 1982.

24. McDonald, J. S., Harty, R. B., and DeBear, W. S., Sodium Heated Steam Generator Test Performance, *Proc. ASME-IEEE Joint Power Generation Conference, New Orleans*, Paper 73-PWR-9, Sept. 16-19, 1983.

DISCLAIMER